

Computational model of the movement of the human muscles of mastication during opening and closing of the jaw

LAETITIA M. M. LEON[†], BERNARD LIEBGOTT^{‡*}, ANNE M. AGUR[‡] and KENNETH H. NORWICH[†]

[†]Institute of Biomaterials & Biomedical Engineering, University of Toronto, Toronto, ON, Canada M5S 1A8

[‡]Division of Anatomy, Department of Surgery, University of Toronto, Toronto, ON, Canada M5S 1A8

(Received 14 June 2006; in final form 12 September 2006)

Muscle fibre bundles comprising the four major muscles of mastication in the human being were studied in cadavers. Markers were placed along each muscle fibre bundle by means of serial dissections. The 3D coordinates of each marker were tabulated and imported to Cinema 4D[®], a software animation program. Origins and insertions of each fibre bundle were also digitized and imported, as were the coordinates of the surface of the skull, the mandible and temporomandibular joint. It was then possible to visualize the movement of all relevant fibre bundles during the passive motions of the mandible. An animated film depicts the positions of all relevant muscle fibres during passive movement of the mandible. The properties of the masseter muscle were documented as a prototype for the eventual study of all the muscles of mastication. One can now proceed to study the inverse problem, namely the forces within each fibre bundle that actively generate mandibular motion. It is hoped that these studies will aid in the management of conditions affecting the temporomandibular joint.

Keywords: 3D reconstruction; Masticatory muscles; Muscle architecture; Computer animation

1. Introduction

The dynamics of the human jaw or mandible are governed by the actions of four primary, bilateral muscles of mastication: *masseter*, *temporalis*, *lateral*, and *medial pterygoid*, (figure 1). During chewing and speech, the mandible both rotates and translates at its primary joint, the *temporomandibular joint (TMJ)*.

Recently, interest has focused on the muscles of mastication due to their possible involvement in TMJ dysfunction (Liu *et al.* 2000). In order to fully appreciate the role of the muscles of mastication in TMJ disorders, it is necessary to develop an in-depth understanding of the functionality and architecture of these muscles. One possible solution is to create a fine-resolution simulation of the muscles of mastication.

Muscle architecture consists of the external shape and internal arrangement of the contractile and connective tissue elements within a muscle (Lieber and Friden 2000). Two muscles that are similar in volume and external appearance may differ functionally due to the internal arrangement of the muscle fibre bundles and tendons. The

muscle cell, also termed the muscle fibre, is 5–15 μm in diameter and can extend the full length of the muscle. Muscle fibres, in turn, are comprised of myofibrils, whose diameters may be less than 1 μm . The myofibrils contain actin and myosin filaments, which are the protein structures that produce the contraction of muscle (figure 2). Muscle fibres are arranged into *fibre bundles*, which are best demarcated with a dissection microscope. Many fibre bundles, in turn, make up muscles, such as masseter or temporalis, whose complex pattern of movements is then determined by the constituent muscle fibre bundles and their orientation.

1.1 Background

A number of investigators have explored these complex movements of the mandible at the level of whole muscle activity. Some were concerned primarily with the forces developed at the mandible (Molnar 1968, Koolstra *et al.* 1988, van Eijden *et al.* 1988). More recent studies by Meyer *et al.* (2000) developed a static simulator of the mandible designed to reproduce the traction forces of the

*Corresponding author. Email: b.liebgott@utoronto.ca

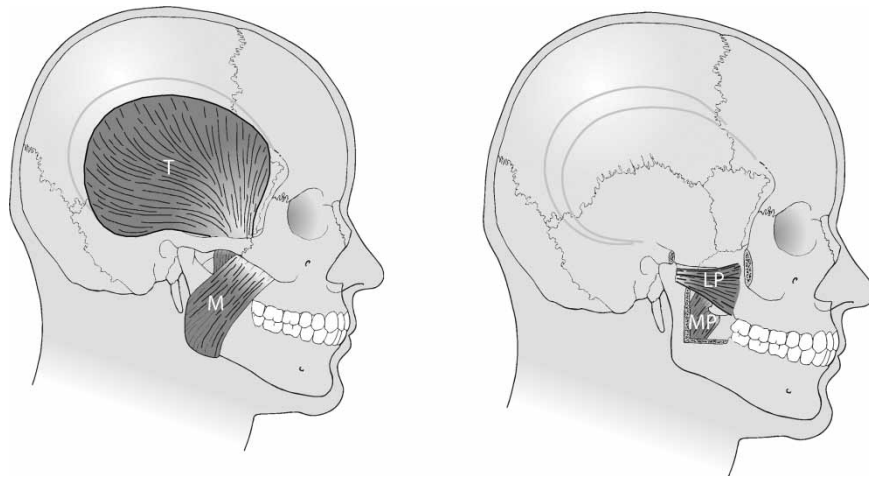


Figure 1. The right muscles of mastication. T, temporalis muscle; M, masseter muscle; MP, medial pterygoid muscle; and LP, lateral pterygoid muscle (from Liebgott B. *Anatomical Basis of Dentistry* 2nd ed. Mosby Inc., 2001).

muscles of mastication. Like many other models, the simulator assumed that muscles are uniformly active and that each muscle can be represented by a line joining the centre of its insertion area to the center of their origin area. Slager *et al.* (1997) represented all the muscles of mastication as one single muscle. Castano *et al.* (2002) used computerized tomography (CT) of a living subject to develop a finite element model of the mandible and TMJ. Total muscle force was distributed using multiple vectors. A number of models of jaw dynamics have attempted to evaluate the roles of the muscles of mastication independently (Langenbach and Hannam 1999, Peck *et al.* 2000). In particular, Koolstra and van Eijden (1995) created a dynamic model of the human masticatory system using the estimated centroids of

origin and insertion for each muscle component to investigate the role of the muscles of mastication in closing the jaw. More studies than we can review here have approximated the forces developed by the muscles of mastication using Hill's model of muscle contraction (Hill 1938). The modeling studies and simulations developed to date are based largely on single or multiple straight lines representing the entire volume of the muscle. Detailed, *in situ*, 3D musculotendinous architecture has not been used for muscle modeling, even though muscle architecture is an important determinant of function (Blemker and Delp 2005).

The muscle fibre bundle length and angle and the number of fibre bundles lying in sequence are important factors in determining the amount of force a muscle is

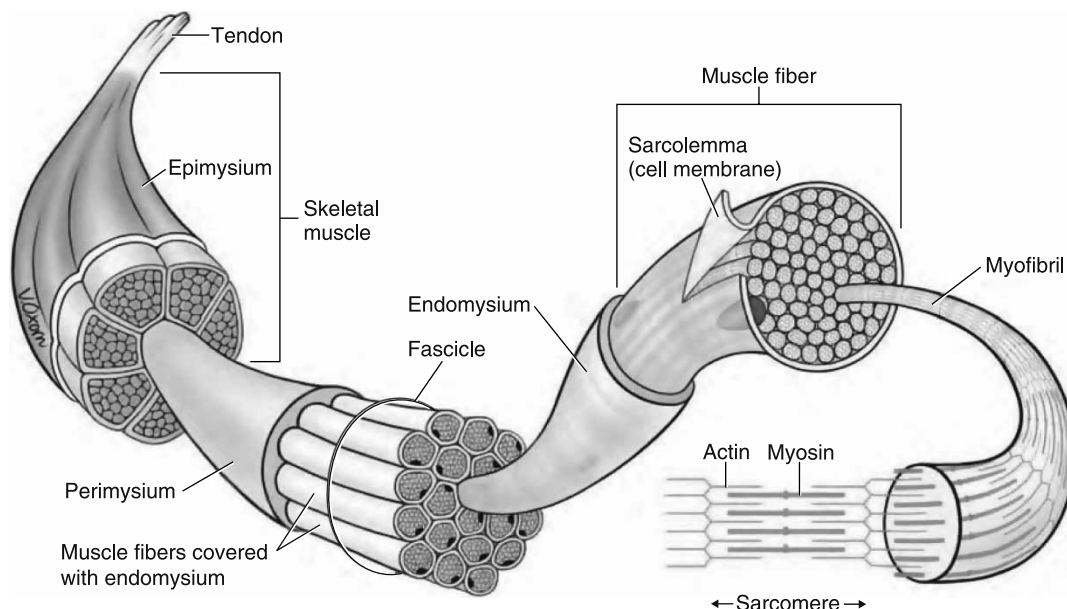


Figure 2. Components of a skeletal muscle illustrating a muscle bundle or muscle fibre. (from Moore, K.L. and Agur, A.M.R. *Essential Clinical Anatomy*, 2nd ed. Lippincott, Williams, and Wilkins, 2002).

capable of producing (Zajac 1989). The architectural parameters have been elucidated using ultrasonographic and 3D cadaveric studies.

In recent years, people have turned to ultrasound to provide images of muscular architecture. However, a study by Gaspard (1993) showed that it was impossible to image the pterygoid muscles by ultrasonography, because of extensive obstacles to the ultrasound wave. Vanneuville *et al.* (1994) concluded that ultrasound imaging was useful primarily as a screening tool and for identifying large tumors or abnormalities, but that CT or MRI were necessary for more detail. So let us briefly review the potential of these two imaging modalities.

CT generates images with excellent resolution and a number of investigators have used it to study the muscles of mastication. Seltzer and Wang (1987) suggested that CT was the modality of choice for imaging lesions of the masseter. Newton *et al.* (1987) used CT to study temporal change in the cross-sectional areas of muscles of mastication with some success. However, CT has its limitations. Like other techniques that employ various scanning planes, some fibres do not appear in the scanned plane due to differences in fibre direction and pennation (Newton *et al.* 1987).

MRI conveys the advantage of use in living systems without the dangers of ionizing radiation and has excellent soft tissue differentiation. Blemker and Delp (2005) used MRI of a live subject to create 3D models with complex muscle geometry for four muscles crossing the hip. However, due to limitations in MRI, the muscle fibres in these models were interpolated from templates and do not correspond to actual muscle fibres. Similar to CT, MRI is again limited by the necessity of image slice selection and as reported by Lieber and Friden (2000), cannot be used to visualize one individual fibre bundle from origin to insertion. Neither can it illustrate variations in length and orientation among various fibre bundles in a muscle.

In order to gain full appreciation of the muscle architecture throughout the volume of a muscle, it is necessary to move beyond conventional imaging techniques. Lemos *et al.* (2004) created a non-linear finite element model of the cat medial gastrocnemius muscle using digital pictures of physical cross-sectional and longitudinal slices of the cat hindlimb. In addition to the external geometry of the muscle, this model also represents the transverse geometry of the cat MG using the shape of 12 fibre bundles, though it falls short of a complete representation of the internal muscle geometry. Agur *et al.* (1999, 2003) and Ng-Thow-Hing *et al.* (2001) used muscle tissue from cadavers to describe a 3D model of individual muscle fibre bundles in the human soleus muscle. Some 400-muscle fibre bundles, located throughout the volume of the muscle, were marked and digitized to generate 3D coordinates, which were then fitted to a B-spline, solid model. This assembly captures the external shape of the muscle as well as the internal fibre architecture throughout the volume of the muscle, permitting a more detailed analysis of the architecture

when compared to existing models. Kertesz *et al.* (2003) used a similar approach to study the architecture of the human lateral pterygoid muscle, one of the primary muscles of mastication, by dissecting and digitizing fibre bundles in the muscles of 19 cadavers. The current work is a further application of the techniques developed by this group.

Therefore, the aims of this study are: (1) to create a working model of the passive movement of the muscles of mastication using fine-resolution, 3D architectural data at the fibre bundle level; and (2) to collect and analyze data from the passive model, to be used in the future development of a dynamic model of the muscles of mastication.

2. Materials and methods

We describe here the process used to collect (*Laboratory techniques*) and analyze (*Computer techniques*) the coordinates of multiple points that lay along the muscle fibre bundles and tendons that make up the four muscles of mastication (masseter, temporalis, lateral and medial pterygoid.).

2.1 Laboratory techniques

Data were collected for the four major muscles of mastication from two, male, formalin embalmed cadaveric specimens, one 73 and one 67 years of age. The skull was fixed on a flat surface to ensure consistency in the coordinates of the muscle fibre bundles. Three screws were inserted into the skull to serve as 3D reference points. In order to ensure that these points were accessible at all times without interfering with the digitization, the screws were placed in the zygomatic arch (side of the face), in the mastoid process (behind the ear) and in the mental foramen (chin). Starting with the masseter muscle, the superficial muscle fibre bundles were identified and delineated with a fine marker, using a dissection microscope. For each fibre bundle, one point was placed at each end of the attachment (origin and insertion), as well as at 6–12 intervening points, to get a good representation of the shape and orientation of the bundle. Next, the muscle fibre bundles were digitized using a MicroScribe-3DX[®] digitizer to record the 3D coordinates of the marked points. When this process had been completed for the superficial fibre bundles, these bundles were removed using a scalpel, to expose the next layer of fibre bundles beneath. This process of serial (layer by layer) dissection was repeated until the muscle was completely digitized. In addition, the outline and a grid of the surface of the tendons to which the fibre bundles attach were digitized. The bony elements (cranium and mandible) and articular disc of the temporomandibular joint were also digitized.

All remaining muscles of mastication were digitized using the same method. In all, hundreds of muscle fibre

bundles were digitized in each of the four primary muscles of mastication. The digitized data were then used to create a static, three-dimensional image of the muscles of mastication and related structures using dynamic animation and control environment software (DANCE) (Ng-Thow-Hing *et al.* 2001).

Having achieved the static imaging, we then proceeded to develop the kinetic image displaying the motions of the individual muscle fibre bundles under passive motion of the mandible.

2.2 Computer techniques

Cinema 4D[®] is software, commercially available, that can be used to generate 3D animation. It consists of a number of *objects* and *expressions* that are clearly described in the operation manual (Becker *et al.* 2002). The Cinema 4D window contains a number of panels and managers that enable the programmer to design, animate and render animations. The view panel allows four separate views at different angles and allows translation, zoom and rotate facilities. We describe here only a few core features of Cinema 4D that will permit the reader to understand how the animation of mastication was achieved.

2.2.1 Null object. This is simply an empty axis system. The null object is useful in animation since other objects can be placed within it.

2.2.2 Polygons. These objects are either triangles (3 points) or quadrangles (4 points). Complex objects can be created from a collection of polygons. The polygon object was used to depict the bony elements of the masticatory system, such as skull and mandible.

2.2.3 Splines. A spline in Cinema 4D is a set of vertices lying in 3D space and connected by either straight lines or curves. For a spline to be visible in an animation, it must be converted to a solid object in the manner described below.

2.2.4 NURBS. NURBS use other objects, such as simple curves, to generate surfaces. *Sweep NURBS* require two splines. For example, to develop the shape of a muscle fibre bundle, the sweep NURB will move the cross section of the fibre bundle along a second spline defining the longitudinal axis of the fibre bundle to create the fibre bundle object. We shall call the cross section spline the *contour spline* and longitudinal axis spline the *path spline*. Another type of NURB called a *HyperNURB*, can be used to round and smooth an object and was used for bony portions of the skull and mandible.

2.2.5 Tags. Tags in Cinema 4D can be attached to objects to assign a particular property to that object. Custom tags

were developed in the C++ programming language to provide the passive movement properties of the muscle fibre bundles. These custom tags will be described below in more detail.

2.2.6 Expressions. Expressions are small programs that assign specific behaviour to objects. There are built-in expressions, custom expressions created by the user and *XPresso* (a Cinema 4D[®] programming language) expressions that can be created without using code. The latter expressions were used together with tags to model the tendons of muscles in the masticatory system.

2.3 Importing data

Data had been collected from the two dissected cadavers and static, 3D images of each of the four muscles of mastication were produced using the DANCE program, described in Section 2.1 above. It was then necessary to import data from DANCE into Cinema 4D. The technical details of the transfer process have been recorded by Leon (2005).

2.3.1 Format for imported data. When the data had been imported successfully into Cinema 4D, a number of objects were created to store the anatomical information. As described in Section 2.2.4, each muscle fibre bundle is described by a *sweep NURBS*. The contour spline representing the cross section of the bundle was described by a circle and the path spline representing the axis of the bundle is a cubic spline created directly from the digitized points. All muscle fibre bundles for a particular muscle layer (or fibreset) were grouped under a null object representing that set. Then all muscle layers (or fibresets) for a particular data file (typically a muscle or portion of a muscle) were grouped under a null object representing that muscle. The object hierarchy in the Object Manager is as follows:

- Muscle_ < muscle_name > (*null object*)
 - FibreSet_ < layer_name1 > (*null object*)
 - Fibre_ < name1 > (*sweep nurb*)
 - circle_ < name1 > (*circle spline*)
 - spline_ < name1 > (*spline*)
 - Fibre_ < name2 > (*sweep nurb*)
 - circle_ < name2 > (*circle spline*)
 - spline_ < name2 > (*spline*).
 - ...
 - FibreSet_ < layer_name2 > (*null object*)
 - Fibre_ < name1 > (*sweep nurb*)
 - circle_ < name1 > (*circle spline*)
 - spline_ < name1 > (*spline*).
 - ...

The origin and insertion points of each of the muscle fibre bundles were handled in much the same way. For each muscle fibre bundle, a null object was created with the

same 3D coordinates as the origin point of the bundle. The origin points for all muscle fibre bundles of a particular muscle layer (or fibreset) were grouped together under a null object representing that layer. Finally, all of the muscle layers (or fibresets) for a particular data file were grouped under a null object representing that muscle. The object hierarchy in the Object Manager is as follows:

- Origin_ < muscle_name > (null object)
 - Origin_FibreSet_ < layer_name1 > (null object)
 - Origin_ < name1 > (null object)
 - Origin_ < name2 > (null object).
 - ...
 - Origin_FibreSet_ < layer_name2 > (null object)
 - Origin_ < name1 > (null object).
 - ...

A similar hierarchy was created for the insertion points of each of the muscle fibre bundles that have been imported.

2.3.2 Digitized skull. The skull (cranium and mandible) grid was digitized from the same cadaver as the muscles of mastication, prior to cutting the skull and dissecting the muscles. Skull data were entered into Cinema 4D in the same manner as muscle fibre bundle data—as a grid composed of Sweep NURBS and splines. In order to create a solid surface, the points of the grid were connected to create a set of polygons and a HyperNURBS object was used to smooth the surface and give the skull a more spherical appearance (please refer to Sections 2.2.2 and 2.2.4). The 3D surface model of the skull is shown in figure 3.



Figure 3. Three-dimensional surface model of the skull created from the digitized grid drawn on the skull surface. A reference plane is shown through the zygomatic arch used to measure the angle of pennation of a digitized muscle bundle (grey) of the masseter muscle.

2.4 Muscle movement

Once the digitized data had been successfully imported into the animation program and the surface models of the skull and mandible had been assembled, the next step was to add movement to the created objects. In a model of the passive movement of the muscles of mastication, movement is applied to the mandible. The muscle fibre bundles were attached to the skull at their respective points of origin and to the mandible at their respective points of insertion. As the mandible moves through a series of positions, the resulting movement of the muscle fibre bundles was documented.

The first step in adding passive movement was to attach the insertion points of the muscle fibre bundles to the mandible. To achieve this in Cinema 4D, the null objects representing the insertion points were made “children” of the mandible (in the object hierarchy in the Object Manager) so that the insertion points maintain the same position and rotation relative to the mandible as the mandible moves. In cases where the muscle fibre bundle is attached to tendon rather than bone, the insertion point was made a “child” of the origin point of the tendon, so that when the tendon moves it pulls the insertion point of the muscle along with it. The next step in the process was to attach the origin points of the muscle fibre bundles to the fixed skull. For each muscle fibre bundle, the null object representing the origin point of this bundle was made a child of the skull object, ensuring that its position relative to the skull remained fixed.

2.4.1 ElasticProperty tag. Once the origin and insertion points of the fibre bundles were anchored, the next step was to model the elastic property of the fibre bundle, which will ensure that the muscle fibre bundle will stretch as an elastic band between origin and insertion points. The “ElasticProperty” tag updates the spline representing the muscle fibre bundle to ensure that it remains in a straight line between origin and insertion as the mandible moves. The ElasticProperty tag also performs collision detection during the period of motion. Collision detection assures that whenever the taut muscle fibre bundle would intersect or “cut” the solid surface of the skull contour, the fibre bundle is, instead, wrapped around the skull contour. Therefore, it was necessary to generate a surface mathematically that would represent the skull contour, a surface that was accurate particularly for the portion of the skull underlying the temporalis muscle, whose fibres are wrapped about the skull. We selected the ellipsoid for this purpose. The ElasticProperty tag was written in C++ code, which we have not reproduced here; however the collision detection algorithm will be described briefly below.

2.4.2 TendonProperty tag. The tendons were treated in a manner similar to that of muscle fibre bundles. The tendon model has a tag, the “Tendon Property” tag, which assigns

properties to them. However, because tendons contain minimal elasticity, they do not behave in the same manner as muscle fibres. Therefore, the TendonProperty tag differs from the ElasticProperty tag in a few ways. First, the TendonProperty tag calculates and stores the initial static length of the tendon fibre bundle. Then, when new coordinates for a point have been calculated using the collision detection algorithm, the TendonProperty tag performs the additional task of rescaling the spline. This rescaling will ensure that the tendon undergoes minimal stretch, which realistically simulates the real tendon. An elasticity parameter is defined. For example, an elasticity parameter of 0.1 limits the stretch of the tendon fibre to 110% of its actual length. The elasticity parameter of a tendon was set to zero. The TendonProperty tag also updates the coordinates of the null object representing the origin point of the tendon to coincide with the coordinates of the last point of the muscle fibre bundle. Code for this tag is also written in C++. An Espresso Expression (Cinema 4D® programming language) was also used in conjunction with the TendonProperty tag to ensure that the coordinates of the null object representing the origin point of the tendon and the coordinates of the last point of the spline remain the same throughout the animation process.

2.5 Collision detection algorithm

This algorithm forms part of the ElasticProperty tag. The lateral aspect of the skull was approximated in three dimensions by an ellipsoid with semi-axes a , b and c say and center $(d, e$ and $f)$. The equation of the ellipsoid is

$$g(x, y, z) = \frac{(x-d)^2}{a^2} + \frac{(y-e)^2}{b^2} + \frac{(z-f)^2}{c^2} = 1 \quad (1)$$

To determine whether or not a collision has occurred between a muscle fibre bundle and the skull, the function $g(u, v, w)$ is evaluated for each point (u, v, w) on the muscle fibre bundle. Then the point falls inside the boundary of the ellipsoid if $g(u, v, w) < 1$ and falls on or outside the boundary if $g(u, v, w) \geq 1$. When the point falls inside the ellipsoid, the tag generates the equation of the straight line between this point and the center of the ellipsoid. The equations defining this straight line are

$$\frac{x-d}{u-d} = \frac{y-e}{v-e} = \frac{z-f}{w-f} \quad (2)$$

Solving equations (1) and (2) yields (for points lying both on the straight line and on the ellipsoid)

$$x = \frac{d + (u-d)t}{t}, \quad y = \frac{e + (v-e)t}{t}, \quad z = \frac{f + (w-f)t}{t} \quad (3)$$

where

$$t = \sqrt{\left(\frac{u-d}{a}\right)^2 + \left(\frac{v-e}{b}\right)^2 + \left(\frac{w-f}{c}\right)^2} \quad (4)$$

Here, x , y and z are the new coordinates to be assigned to the colliding point of the spline. This process has the effect of moving the colliding point outwards along the straight line joining this point with the center of the ellipsoid, until it reaches the surface of the ellipsoid. It is repeated for each point of the spline, thus ensuring that there is no collision between the muscle fibre bundles and the ellipsoid representing the skull. Hence, the muscle fibre bundles do not appear to be cutting through the skull in the animated model.

2.6 Mandible movement algorithm

The final step in simulating the physical process of mastication is to introduce the movement of the mandible, particularly the passive opening movement of the mandible. As the mandible moves from the closed position to the wide gape position, the axis of rotation about which the mandible rotates varies. From the normal occluded position, the initial 20–27 mm of interincisal opening occurs through a horizontal axis of rotation through the condyles (Liebgott 2001). Next, the condyles and articular discs translate downward and forward along the articular eminences. Maximal opening of the jaw is achieved when the condyles and discs sit atop the articular eminences. As the condyles encounter the posterior slope of the articular eminences, the instantaneous axis of rotation shifts from the condyles to approximately the midpoint of the mandibular ramus (Grant 1973). It is important to note that continuous rotation through the initial condylar axis would cause the mandible to collide with the vertebral unit posteriorly.

To simulate the movement of the mandible in Cinema 4D, the Timeline manager was used. The mandible was manually moved through the different positions and the coordinates and rotation values of the mandible were recorded to create the animation. The animation of the jaw opening procedure lasts 45 frames, with the first 20 frames representing the initial rotation from the rest position and the remaining frames representing the movement along the eminence and the shifting axis of rotation.

When the above steps had been completed, a QuickTime® animation of the passive movement model was created using Cinema 4D's rendering abilities. This type of animation file is in a common format, which can be included in virtual slide presentations and run on most computer systems. The closing phase of passive mandibular motion was approximated by playing the data back in reverse order. An "AnimateFibre" tag, written in C++, was used to control the animation of the jaw closing process. Following this step, it was possible to view and analyze the created simulation model.

2.7 FibreProperties tag

A third tag called the “FibreProperties” tag was created in C++. This tag has four modifiable parameters. The first parameter, *output frequency*, specifies the frequency (in number of frames) with which the data should be recorded and output. For example, if output frequency is set to 3, then the data will be recorded every third frame throughout the length of the animation. The second parameter, *output length*, is a Boolean value which determines whether or not the length of the fibre bundles will be output when the data are recorded. The third parameter, *output angle*, is another Boolean value which determines whether or not the fibre bundle angle will be output when the data are recorded. The fourth parameter for this tag, *angle reference line*, specifies the direction from which the fibre bundle angle is calculated. If two muscle fibre bundles in three-space are represented by the vectors **A** and **B**, the angle contained between them is given by the usual

$$\cos \theta = \frac{\mathbf{A} \cdot \mathbf{B}}{(|\mathbf{A}| |\mathbf{B}|)}. \quad (5)$$

For the purpose of this article, we will define the angle of a muscle fibre bundle in terms of the angle it forms with a line through the zygomatic arch (figure 3).

The properties of the deep and superficial portions of the masseter muscle were recorded and analyzed, although the same procedure could be repeated for the remaining muscles of mastication.

3. Results and analysis

A number of animation files were created simulating the passive movement of the muscles of mastication during the opening (depression) and closing (elevation) of the mandible. The movies were rendered as QuickTime® movies and can be viewed using the QuickTime player, a commercially available software application. A separate simulation was created for each of the four muscles of mastication, as well as one animation file depicting the four muscles of mastication working together. In the case of the medial pterygoid muscle, the mandible was hidden when rendering the animation, to enable the viewing of the muscle fibre bundles that would otherwise have been hidden. Each movie contains 90 frames (45 frames each for the opening and closing of the mandible) and was rendered at a frame rate of 30 frames per second, producing simulations of 3 s in duration. The movies can then be looped (using the QuickTime Player) to give the appearance of continuous opening and closing movements of the mandible. Figure 4 captures frames 0 (maximum intercuspal contact), 20 (maximum hinge opening) and 45 (maximum or wide open position) for each of the four muscles of mastication.

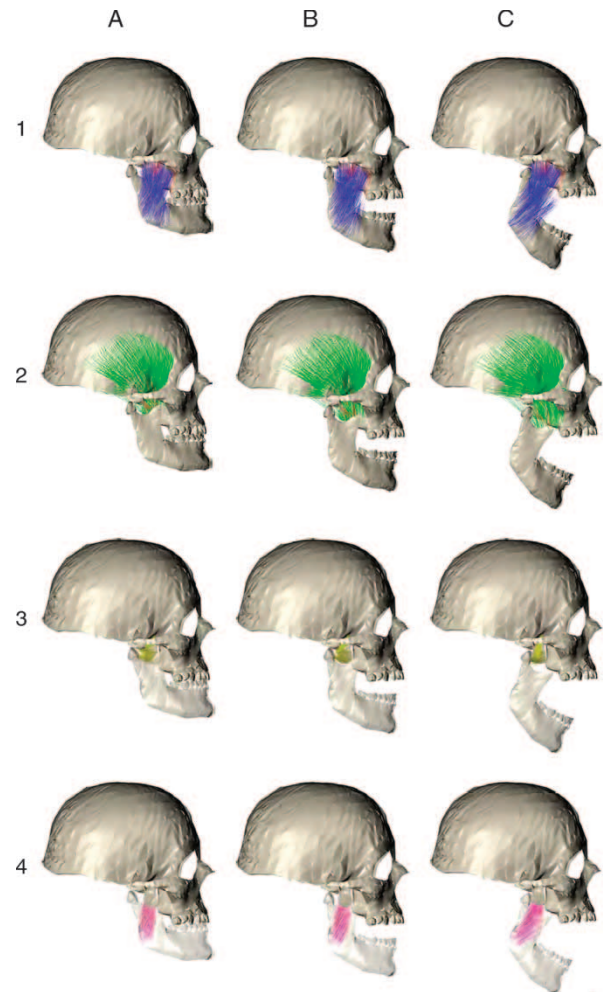


Figure 4. (1) Animation depicting the movements of the muscle fibre bundles of the masseter muscle (blue). (A) Frame 0, maximum intercuspal position; (B) frame 20, maximum hinge rotation; and (C) frame 45, maximum opening. (2) Animation depicting the movements of the muscle fibre bundles of the temporalis muscle (green). (A) Frame 0, maximum intercuspal position; (B) frame 20, maximum hinge rotation; and (C) frame 45, maximum opening. (3) Animation depicting the movements of the muscle fibre bundles of the lateral pterygoid muscle (yellow). (A) Frame 0, maximum intercuspal position; (B) frame 20, maximum hinge rotation; and (C) frame 45, maximum opening. (4) Animation depicting the movements of the muscle fibre bundles of the medial pterygoid muscle (purple). (A) Frame 0, maximum intercuspal position; (B) frame 20, maximum hinge rotation; (C) frame 45, maximum opening.

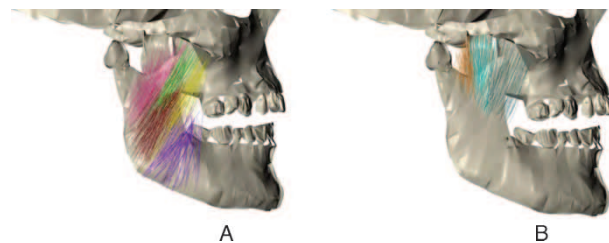


Figure 5. (A) Screen shot depicting the categorization of the muscle fibre bundles for the deep portion of the masseter muscle. Division 1 (orange) represents the posterior portion, division 2 (aqua) represents the middle portion and division 3 represents the anterior portion. (B) Screen shot depicting the categorization of the muscle fibre bundles for the superficial portion of the masseter muscle. Division 1 (pink) represents the posterior portion of the muscle, division 2 (green) the superomedial portion of the muscle, division 3 (brown), the inferomedial portion of the muscle, division 4 (yellow), the anterosuperior portion and division 4 (purple), the anteroinferior portion.

3.1 Muscle length and angle tracking

Muscle fibre bundle length and angle of pennation were recorded using the FibreProperties tag and were thence exported to an Excel[®] spreadsheet. The complete set of properties for the masseter muscle can be found elsewhere (Leon 2005). However, a summary containing mean, maximum and minimum values for length and angle of pennation for the muscle fibre bundles of the deep masseter can be found in tables 1(a) and (b).

Large quantities of data defining the properties of fibre bundles of the muscles of mastication during passive movement of the mandible can be tabulated and accessed in this fashion. However, one goal of the present research is to enable the modeling of the active phase of mandibular

movement during mastication. The modeling of the active phase cannot likely begin at the level of individual muscle fibre bundles, but may proceed by considering a group of muscle fibre bundles.

To simplify analysis, we have divided both the deep and superficial portions of the masseter muscle into divisions and have calculated the average fibre bundle length and angle of pennation of each division (tables 1–4). These divisions were chosen based on the origin and insertion points of the fibre bundles. The fibre bundles of the deep masseter muscle were divided into three divisions (figure 5(a)) and the fibre bundles of the superficial masseter muscles were divided into five divisions (figure 5(b)).

Table 1. Average, maximum and minimum lengths (mm) of the muscle fibre bundles of the deep masseter muscle recorded every fifth frame throughout the 45 frame animation. Frame 0 represents maximal intercusp contact; frame 20 represents end of hinge rotation; and frame 45 represents maximal open position.

Length (mm)	Frame									
	0	5	10	15	20	25	30	35	40	45
Average	26.49	27.47	28.82	30.54	32.66	35.17	37.95	40.27	41.99	42.85
Maximum	41.92	44.02	46.51	47.93	49.62	51.51	53.51	56.90	59.41	60.68
Minimum	10.81	11.25	11.84	12.76	13.92	15.21	16.55	17.65	18.43	18.81

Table 2. Average, maximum and minimum angles of pennation (°) of the muscle fibre bundles of the deep masseter muscle recorded every fifth frame throughout the 45 frame animation. Frame 0 represents maximal intercusp contact; frame 20 represents end of hinge rotation; and frame 45 represents maximal open position.

Angle (°)	Frame									
	0	5	10	15	20	25	30	35	40	45
Average	85.84	84.74	83.60	83.66	83.90	82.97	81.39	79.81	78.49	77.76
Maximum	113.45	111.27	108.69	107.03	107.09	105.77	103.88	102.10	100.73	100.04
Minimum	62.97	62.51	62.11	62.74	63.48	63.25	62.28	61.13	60.05	59.42

Table 3. Average, maximum and minimum lengths (mm) of the muscle fibre bundles of the superficial masseter muscle recorded every fifth frame throughout the 45 frame animation. Frame 0 represents maximal intercusp contact; frame 20 represents end of hinge rotation; and frame 45 represents maximal open position.

Length (mm)	Frame									
	0	5	10	15	20	25	30	35	40	45
Average	30.16	31.40	33.20	35.22	37.53	40.85	44.84	48.25	50.64	51.83
Maximum	60.78	62.37	64.41	66.60	69.02	72.20	75.64	80.28	82.33	83.33
Minimum	9.20	10.09	11.35	13.44	16.11	19.10	21.11	22.61	23.44	23.84

Table 4. Average, maximum and minimum angles of pennation (°) of the muscle fibre bundles of the superficial masseter muscle recorded every fifth frame throughout the 45 frame animation. Frame 0 represents maximal intercusp contact; frame 20 represents end of hinge rotation; frame 45 represents maximal open position.

Angle (°)	Frame									
	0	5	10	15	20	25	30	35	40	45
Average	51.61	67.79	66.52	65.05	64.13	63.19	61.08	58.06	55.10	52.82
Maximum	74.83	116.54	106.17	99.64	94.48	89.50	82.56	79.81	77.58	75.80
Minimum	27.62	47.78	45.66	43.66	43.20	42.86	39.82	35.70	31.97	29.11

In tables 5–7 are given the data for mean fibre bundle length, mean fractional increase in length and mean angles of pennation for each of the three divisions of the deep masseter muscle. Similarly, tables 8–10 show the data for mean fibre bundle length, mean fractional increase in length and mean angles of pennation for each of the five divisions of the superficial head of the masseter muscle. In a first order model of the active process, each of these

Table 5. Average lengths (mm) of the muscle fibre bundles recorded every fifth frame throughout the 45 frame animation. Data are shown for each of the three divisions of the deep masseter muscle.

Division	Frame									
	0	5	10	15	20	25	30	35	40	45
1	20.7	21.24	22.02	23.19	24.71	26.29	27.94	29.31	30.29	30.77
2	26.5	27.28	28.47	30.14	32.36	34.74	37.39	39.45	40.95	41.71
3	29.8	31.13	32.90	34.96	37.35	40.48	43.99	47.03	49.3	50.45

Table 6. Average angles of pennation (°) of the muscle fibre bundles recorded every fifth frame throughout the 45 frame animation. Data are shown for each of the three divisions of the deep masseter muscle.

Division	Frame									
	0	5	10	15	20	25	30	35	40	45
1	96.62	95.29	93.90	94.05	94.47	93.63	92.23	90.82	89.68	89.06
2	93.74	92.66	91.43	91.14	91.00	89.77	87.86	86.07	84.61	83.82
3	74.35	73.38	72.43	72.68	73.08	72.30	70.86	69.32	67.99	67.25

Table 7. Average lengths (mm) of the muscle fibre bundles recorded every fifth frame throughout the 45 frame animation. Data are shown for each of the five divisions of the superficial masseter muscle.

Division	Frame									
	0	5	10	15	20	25	30	35	40	45
1	26.07	26.91	28.06	29.34	30.76	32.73	34.97	36.87	38.24	38.91
2	31.76	32.67	34.24	36.13	38.31	41.73	46.18	49.84	52.15	53.26
3	32.05	33.31	34.99	36.77	38.76	41.55	44.77	47.53	49.55	50.55
4	36.68	38.27	40.48	42.94	45.72	49.66	54.36	58.35	61.18	62.56
5	26.24	28.01	30.40	33.08	36.15	40.37	45.28	49.62	52.92	54.63

Table 8. Average angles of pennation (°) of the muscle fibre bundles recorded every fifth frame throughout the 45 frame animation. Data are shown for each of the five divisions of the superficial masseter muscle.

Division	Frame									
	0	5	10	15	20	25	30	35	40	45
1	66.90	66.39	65.77	65.72	65.75	64.94	63.50	61.94	60.59	59.84
2	64.12	63.70	63.08	62.44	61.53	59.33	55.58	51.70	48.87	47.40
3	63.25	63.26	63.08	62.91	62.77	62.23	61.20	59.96	58.85	58.22
4	66.13	65.58	64.83	64.43	63.96	62.47	60.07	57.58	55.59	54.52
5	76.34	72.21	67.78	64.97	62.37	57.99	52.99	48.68	45.43	43.74

Table 9. Average percent increases in length of the muscle fibre bundles shown for each frame interval (e.g. frames 0–5). Data are given for each of the three divisions of the deep head of the masseter muscle.

Division	Frame									
	0–5 (%)	5–10 (%)	10–15 (%)	15–20 (%)	20–25 (%)	25–30 (%)	30–35 (%)	35–40 (%)	40–45 (%)	
1	2.51	3.63	5.35	6.53	6.39	6.30	4.90	3.34	1.59	
2	3.09	4.37	5.89	7.34	7.37	7.62	5.50	3.82	1.85	
3	4.53	5.71	6.26	6.82	8.37	8.67	6.91	4.83	2.35	

Table 10. Average percent increases in length of the muscle fibre bundles shown for each frame interval (e.g. frames 0–5). Data are given for each of the five divisions of the superficial head of the masseter muscle.

Division	Frame								
	0–5 (%)	5–10 (%)	10–15 (%)	15–20 (%)	20–25 (%)	25–30 (%)	30–35 (%)	35–40 (%)	40–45 (%)
1	3.22	4.30	4.54	4.87	6.40	6.84	5.42	3.71	1.76
2	2.85	4.82	5.51	6.05	8.91	10.67	7.93	4.64	2.12
3	3.92	5.04	5.08	5.41	7.20	7.75	6.18	4.24	2.02
4	4.35	5.77	6.06	6.48	8.63	9.46	7.34	4.84	2.26
5	6.73	8.54	8.82	9.26	11.69	12.15	9.59	6.64	3.23

three units may be regarded as a single unit of muscular contraction, invested with the measured properties. These tabular values can, of course, be graphed for easier visualization. Mean fibre bundle lengths for each division of the deep head of masseter (data of table 2(a)) are graphed in figure 6(a) and those of the superficial head in figure 6(b). In the active model, we are concerned more with the elevation of the mandible, which is nearest to the passive model in reverse (mandible depression). However, one must also be concerned here with the phenomenon of elastic hysteresis, whereby the stress–strain relationships in the active elevation of the mandible will deviate from their analogs in passive depression of the mandible. Still,

using the process of grouping muscle fibre bundles into divisions, we have a start toward the active model.

4. Discussion

4.1 Difficulties encountered in producing this model

Bearing in mind that thousands of manually digitized coordinates obtained from cadavers had to be incorporated into this computer animation, some difficulties and inconsistencies were not unexpected.

The 3D surface model of the skull was constructed from a manually digitized grid of the skull surface. However, due to precision limitations in the digitization procedure, the horizontal and vertical lines of this grid did not always intersect precisely in three-space. Therefore, in constructing the skull surface within Cinema 4D, it was sometimes difficult to determine which points should be connected in polygons, which limited the accuracy of the skull object.

Another problem involved specification of the muscle fibre bundle insertions. It was often difficult to discern whether the bundles inserted into a tendon, or directly into the mandible. Such insertion points are much easier to detect directly from a cadaver than from the static, three-dimensional image encoded in the DANCE software.

Still, all in all, the creation of the simulation proceeded smoothly.

4.2 Validation of the model

A number of the assumptions made in constructing the model cannot be validated by direct means. For example, all muscle fibre bundles were approximated by straight lines that extend from origin to insertion points. As a fibre bundle must be taut to generate a force, the straight line approximation is believed to be reasonable. Other simplifications were introduced, for example, by modeling the muscle tendons as inextensible elements. The TendonProperty tag permits the specification of tendon elasticity, which was set to 0%. This assumption seems reasonable, following measurements made by Curwin and Stanish (1984), where tendons were shown to change their lengths by less than 4%. However, two facets of the model may, indeed, be validated in part with reference to published experimental data. We examine first the

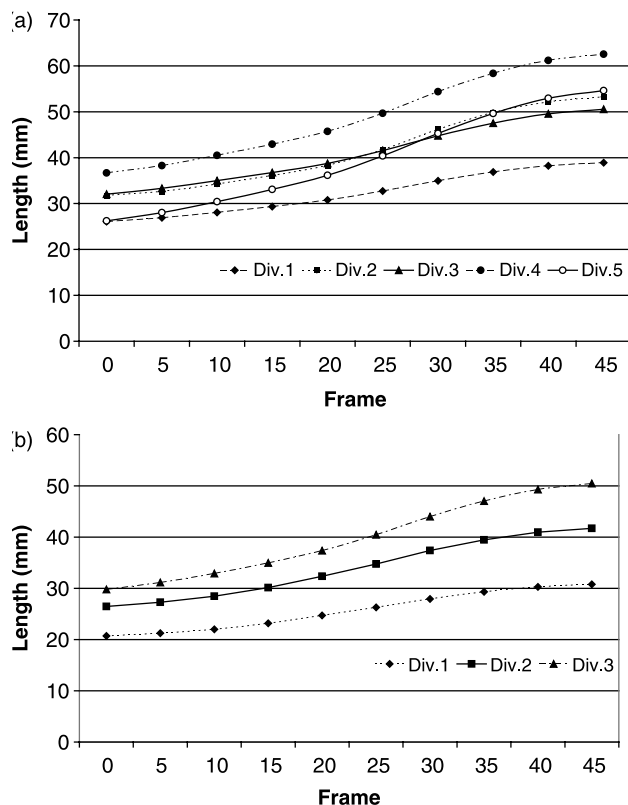


Figure 6. Graph of average lengths (mm) of the muscle fibre bundles for each frame of the animation. Data are given for each of the: (a) five divisions of the superficial head of the masseter muscle; and (b) three divisions of the deep head of the masseter muscle.

movement of the mandible; then the movements of individual muscle fibre bundles.

4.2.1 Validation of mandibular motion. Peck *et al.* (2000) have described the various positions of the mandible numerically. For example, during jaw opening (depression of the mandible), the initial hinge rotation is described as a 13° rotation in the sagittal plane. It was observed that this movement produces a 20 mm vertical translation, resulting in a 20 mm interincisal distance (between the upper and lower central incisor teeth). In addition, the movement following the hinge rotation is described by a 17° sagittal plane rotation and a 16 mm anterior translation. This movement produces a 30 mm vertical translation, resulting in an interincisal distance of 50 mm at the wide-gape position. Thus, an accurate model of the depression of the mandible must closely reproduce these movements.

In our model, as mentioned above, the mandible was manually moved through a series of known positions. We then measured the amount of rotation and the interincisal distances at each step, in order to validate this movement using the documented measurements by Peck *et al.* (2000). In our model, a rotation of 13° about an intercondylar axis was applied to the mandible during the first 20 frames of animation (hinge rotation). At frame 20, the interincisal distance was measured to be approximately 19 mm, which is close to the 20 mm specified by Peck *et al.* During the following frames, the mandible was rotated a remaining 17°, to give a total rotation of 30°. In addition, a translation was applied to the mandible so that the condyle rested on the articular eminence by the end of the final frame, 45. The length of this translation was determined to be approximately 17 mm, which is reasonably close to the 16 mm translation of Peck *et al.* Finally, the interincisal distance at frame 45 was measured to be approximately 52 mm, again in line with the required 50 mm. Therefore, the passive movements of the modeled mandibular depression seem to be quite accurate.

4.2.2 Validation of muscle fibre bundle movement.

Clearly, validation of fibre bundle lengths is more complex than validation of mandibular movement, because very few relevant measurements of muscle fibre lengths appear in the literature. However, some indirect comparisons are still available.

Peck *et al.* (2000) confirmed that the muscles of mastication attain their maximum lengths at the wide gape position and that maximum length corresponds to approximately 150% of optimal length (the mandibular position for maximum bite force). Langenbach and Hannam (1999) conclude that a realistic model can be obtained when optimal fibre lengths correspond to an interincisal distance of 12 mm.

In our model, a 12 mm interincisal distance is attained approximately at frame 10, which we take as optimal and the wide-gape position is reached at frame 45. The fibre

bundles of the deep masseter muscle have a mean length of 28.82 mm at frame 10 (optimal length) and a mean length of 42.85 mm at frame 45 (maximum length), representing an increase in length of 149%. The fibre bundles of the superficial masseter muscle have a mean length of 33.2 mm at frame 10 (optimal length) and a mean length of 51.83 mm at frame 45 (maximum length), representing an increase in length of 156%. Thus, we see that the fractional increase in fibre length from frame 10 (optimal length) to frame 45 (maximum length) corresponds closely to the expected value of 150%.

4.3 Novelty and potential of the model

The simulation developed here models the passive movement of the muscles of mastication with fibre bundle resolution. Each of the four major muscles of mastication has been represented in the simulation by the hundreds or thousands of muscle fibre bundles that constitute it. Hence, we are able to study movements of these muscles with precision not before possible. The model permits us to record and analyze measurements of fibre bundle length and fibre bundle angle with detail not possible using other methods of imaging. The data may lead to improved understanding of the individual and conjoint functioning of the muscles of mastication.

Tabulation of data has been reported only for the masseter muscle, although all four muscles have been digitized. We anticipate that similar studies can be carried out on the remaining three muscles.

Future work will include volume preservation in muscle fibre bundles, to ensure that the volumes of contracted and extended muscle fibres occupy constant volumes. Allowance must also be made for other movements of the mandible, such as lateral movements, protrusion and retrusion (forward and backward movements).

The most important feature of the present work is its potential in aiding construction of a model of active fibre bundle contraction, in which the forces, angles and timing of muscle fibre bundle contractions can be integrated to produce an accurate description of elevation of the mandible during mastication. Forces developed in individual muscle fibre bundles would be summated vectorially to produce the resultant motion. This active model would describe normal movement of the mandible, but would presumably operate under abnormal circumstances as well. For example, an active movement model could allow for selective activation of particular muscle fibre bundles, while other fibre bundles remain uncontracted.

As mentioned above, TMJ disorders are prevalent and sometimes poorly understood. They are believed to be caused by improper functioning of the muscles of mastication. Using an active movement model, one can try to simulate TMJ malfunction, perhaps to identify those muscle fibre bundles that are contracting improperly or out of time sequence. Targeting these muscle fibre bundles is a potentially useful therapeutic device. The current passive

model does not, in its present form, permit this sort of investigation, but it is a necessary stepping-stone to that end.

5. Conclusions

A passive movement model of individual muscle fibre bundles comprising the four major muscles of mastication has been produced. The result is a computer-generated animation of mastication and tabulation of a great deal of data regarding muscle fibre lengths and angles of pennation during the masticatory process, particularly for the masseter muscle. The first step has been taken toward producing a model involving active contraction of individual muscle fibres in the muscles of mastication, a model of some importance in the diagnosis and treatment of disorders of the temporomandibular joint.

Acknowledgements

This work has been supported by a Discovery Grant from the Natural Sciences and Engineering Research Council of Canada to K. H. Norwich and by an NSERC postgraduate award to L. Leon.

References

- A. Agur, K. Ball, V. Ng, R. Leekam, E. Fiume and N. McKee, "The human soleus muscle: a dynamic 3D model", *Clin. Anat.*, 12, p. 199, 1999.
- A. Agur, V. Ng-Thow-Hing, K. Ball, E. Fiume and N.H. McKee, "Documentation and three-dimensional modeling of human soleus muscle architecture", *Clin. Anat.*, 16, pp. 285–293, 2003.
- O. Becker, A. von Koenigsmarck, D. Link, S. Marriott, M. O'Neill, D. O'Reilly, J. Pauke, P. Stacy and J. Walker, *Cinema 4D Reference Manual: 3D for the Real World*, Bedford: Maxon Computer Ltd., 2002.
- S.S. Blemker and S.L. Delp, "Three dimensional representation of complex muscle architectures and geometries", *Ann. Biomed. Eng.*, 33(5), pp. 661–673, 2005.
- M.C. Castano, U. Zapata, A. Pedroza, J.D. Jaramillo and S. Roldan, "Creation of a three-dimensional model of the mandible and the TMJ *in vivo* by means of the finite element method", *Int. J. Comput. Dent.*, 5, pp. 87–99, 2002.
- M. Gaspard, "Exploration structurale et fonctionnelle du complexe musculaire temporo-masseterin par la tomoechographie", *Cah. Prothese.*, 81, pp. 37–73, 1993.
- P.G. Grant, "Lateral pterygoid: two muscles?", *Am. J. Anat.*, 138, pp. 1–9, 1973.
- A.V. Hill, "The heat of shortening and the dynamic constant of muscle", *Proc. Roy. Soc. B*, 126, pp. 136–195, 1938.
- T. Kertesz, B. Liebgott, C.M.L. Clokie and A. Agur, "Poster 6: Architecture of the human lateral pterygoid muscle: a novel 3-dimensional analysis", *J. Oral Maxillofac. Surg.*, August 61(Supplement), pp. 83–84, 2003.
- J.H. Koolstra, T.M. van Eijden, W.A. Weijs and M. Naeije, "A three-dimensional mathematical model of the human masticatory system predicting maximum possible bite forces", *J. Biomech.*, 21, pp. 563–576, 1988.
- J.H. Koolstra and T.M. van Eijden, "Biomechanical analysis of jaw-closing movements", *J. Dent. Res.*, 74, pp. 1564–1570, 1995.
- G.E. Langenbach and A.G. Hannam, "The role of passive muscle tensions in a three-dimensional dynamic model of the human jaw", *Arch. Oral Biol.*, 44, pp. 557–573, 1999.
- R.R. Lemos, M. Epstein, W. Herzog and B. Wyvill, "A framework for structured modeling of skeletal muscle", *Comput. Methods Biomech. Biomed. Eng.*, 7(6), pp. 305–317, 2004.
- L.M.M. Leon, "A functional, three-dimensional reconstruction of the human masticatory system", MSc. thesis, University of Toronto 2005.
- R. Lieber and J. Friden, "Functional and clinical significance of skeletal muscle architecture", *Muscle Nerve*, 23, pp. 1647–1666, 2000.
- B. Liebgott, *The Anatomical Basis of Dentistry*, 2nd ed., St Louis: Mosby, 2001, pp. 292–308.
- Z. Liu, K. Yamagata, K. Kuroe, S. Suengaga, T. Noikura and G. Ito, "Morphological and positional assessments of TMJ components and lateral pterygoid muscle in relation to symptoms and occlusion of patients with temporomandibular disorders", *J. Oral Rehabil.*, 27, pp. 860–874, 2000.
- C. Meyer, J.L. Kahn, A. Lambert, P. Boutemy and A. Wilk, "Development of a static simulator of the mandible", *J. Craniomaxillofac. Surg.*, 28, pp. 278–286, 2000.
- S. Molnar, "Mechanical simulation of human chewing motions", *J. Dent. Res.*, 47, pp. 559–563, 1968.
- J. Newton, R. Abel, E. Robertson and R. Yemm, "Changes in human masseter and medial pterygoid muscles with age: a study by computer tomography", *Gerodontics*, 3, pp. 151–154, 1987.
- V. Ng-Thow-Hing, A. Agur and N. McKee, "A muscle model that captures external shape, internal fibre architecture and permits simulation of active contraction with volume preservation", *Proceedings of the Fifth International Symposium of Computer Models in Biomechanics and Biomedical Engineering*, 2001.
- C.C. Peck, G.E. Langenbach and A.G. Hannam, "Dynamic simulation of muscle and articular properties during human wide jaw opening", *Arch. Oral Biol.*, 45, pp. 963–982, 2000.
- S.E. Seltzer and A.M. Wang, "Modern imaging of the masseter muscle: normal anatomy and pathosis on CR and MRI", *Oral Surg. Oral Med. Oral Pathol.*, 63, pp. 622–629, 1987.
- G.E. Slager, E. Otten, T.M. van Eijden and J.D. van Willigen, "Mathematical model of the human jaw system simulating static biting and movements after unloading", *J. Neurophysiol.*, 78, pp. 3222–3233, 1997.
- G. Vanneville, G. Birou, P. Deloup, M. Guillot, A. Boissier and J. Garcier, "The anatomical basis for ultrasonography of the lateral pterygoid muscle and the infratemporal fossa", *Surg. Radiol. Anat.*, 16, pp. 57–61, 1994.
- T.M. van Eijden, E.M. Klok, W.A. Weijs and J.H. Koolsta, "Mechanical capabilities of the human jaw muscles studied with a mathematical model", *Arch. Oral Biol.*, 33, pp. 819–826, 1988.
- F.E. Zajac, "Muscle and tendon: properties, models, scaling, and application to biomechanics and motor control", *CRC Crit. Rev. Biomed. Eng.*, 17, pp. 359–411, 1989.